Physics Letters B 807 (2020) 135596

Contents lists available at ScienceDirect

Physics Letters B

www.elsevier.com/locate/physletb

g-factor and static quadrupole moment for the wobbling mode in ^{133}La

Q.B. Chen [a,*], S. Frauendorf [b], N. Kaiser [a], Ulf-G. Meißner [c,d,e], J. Meng [f,g]

[a] Physik-Department, Technische Universität München, D-85747 Garching, Germany
[b] Physics Department, University of Notre Dame, Notre Dame, IN 46556, USA
[c] Helmholtz-Institut für Strahlen- und Kernphysik and Bethe Center for Theoretical Physics, Universität Bonn, D-53115 Bonn, Germany
[d] Institute for Advanced Simulation, Institut für Kernphysik and Jülich Center for Hadron Physics, Forschungszentrum Jülich, D-52425 Jülich, Germany
[e] Ivane Javakhishvili Tbilisi State University, 0186 Tbilisi, Georgia
[f] State Key Laboratory of Nuclear Physics and Technology, School of Physics, Peking University, Beijing 100871, China
[g] Yukawa Institute for Theoretical Physics, Kyoto University, Kyoto 606-8502, Japan

ARTICLE INFO

Article history:
Received 30 May 2020
Received in revised form 20 June 2020
Accepted 25 June 2020
Available online 30 June 2020
Editor: W. Haxton

ABSTRACT

The g-factor and static quadrupole moment for the wobbling mode in the nuclide ^{133}La are investigated as functions of the spin I by employing the particle rotor model. The model can reproduce the available experimental data of the g-factor and static quadrupole moment. The properties of the g-factor and static quadrupole moment as functions of I are interpreted by analyzing the angular momentum geometry of the collective rotor, proton-particle, and total nuclear system. It is demonstrated that the experimental value of the g-factor at the bandhead of the yrast band leads to the conclusion that the rotor angular momentum is $R \simeq 2$. Furthermore, the variation of the g-factor with the spin I yields the information that the angular momenta of the proton-particle and total nuclear system are oriented parallel to each other. The negative values of the static quadrupole moment over the entire spin region are caused by an alignment of the total angular momentum mainly along the short axis. Differences of the static quadrupole moment between the wobbling and yrast band originate from a wobbling excitation with respect to the short axis.

© 2020 The Author(s). Published by Elsevier B.V. This is an open access article under the CC BY license (http://creativecommons.org/licenses/by/4.0/). Funded by SCOAP[3].

The collective motions of a triaxially deformed nucleus, that is shaped like an ellipsoid with three principal axes of inertia, have attracted a lot of attention in nuclear structure physics over the last years. When such a nucleus rotates, the lowest energy state for a given angular momentum I (called yrast state) corresponds to a uniform rotation about the principal axis with the largest moment of inertia (MoI). At a slightly higher excitation energy, this axis can execute a precession motion (in the form of a harmonic oscillation) about the space-fixed angular momentum vector. This describes the phenomenon of the so-called wobbling motion that has been first proposed by Bohr and Mottelson in the 1970s [1]. Since this collective mode is a rotation about a principal axis, the related energy spectra come as a series of rotational $\Delta I = 2$ bands, in which the signature of the bands alternates with increasing number of oscillation quanta n. The electric quadrupole transitions with $\Delta I = 1$ and $n \to n - 1$ are induced by a wobbling motion of the entire charged rigid body, and thus get collectively enhanced.

Recent studies of the nuclear wobbling motion have been triggered by the novel concepts of *transverse* wobbling (TW) and *longitudinal* wobbling (LW) proposed by Frauendorf and Dönau [2]. These authors have classified the wobbling modes in the presence of a high-j quasi-particle according to the relative orientation of the angular momentum of the quasi-particle $\boldsymbol{j}_p$ and the principal axis with the largest MoI, which is usually the intermediate axis. If this relative orientation is perpendicular, one speaks of a *transverse* wobbling mode, and the corresponding wobbling energy decreases with the spin I. It has been observed experimentally for the nuclei ^{161}Lu [3], ^{163}Lu [4,5], ^{165}Lu [6], ^{167}Lu [7], and ^{167}Ta [8] in the $A \approx 160$ mass region, for the nuclides ^{135}Pr [9,10] and ^{130}Ba [11–13] in the $A \approx 130$ mass region, and for the odd-neutron nuclide ^{105}Pd [14] in the $A \approx 100$ mass region. If the relative orientation is parallel, one speaks of a *longitudinal* wobbling mode, where the wobbling energy increases with the spin I. The experimental evidence for longitudinal wobbling is, however, rare and has only been reported very recently for the nuclides ^{133}La [15] and ^{187}Au [16].

The increase of the wobbling energy with the spin I for the nucleus ^{133}La is quite unexpected, because the wobbling mode is based on the configuration $\pi(1h_{11/2})^1$ with an orientation of the

* Corresponding author.
E-mail addresses: qbchen@pku.edu.cn (Q.B. Chen), sfrauend@nd.edu (S. Frauendorf), nkaiser@ph.tum.de (N. Kaiser), meissner@hiskp.uni-bonn.de (U.-G. Meißner), mengj@pku.edu.cn (J. Meng).

https://doi.org/10.1016/j.physletb.2020.135596
0370-2693/© 2020 The Author(s). Published by Elsevier B.V. This is an open access article under the CC BY license (http://creativecommons.org/licenses/by/4.0/). Funded by SCOAP[3].

$h_{11/2}$ proton along the short axis [15]. The same $h_{11/2}$ proton configuration applies to the isotones ^{135}Pr [9,10] and ^{131}Cs [31], which both show a decrease of the wobbling energy with the spin I, and this behavior is actually a hallmark of the transverse wobbling mode. The authors of Ref. [15] have explained the unexpected increase of the wobbling energy with spin I for ^{133}La as follows. Like the isotones, this nucleus is triaxially deformed and thus it features the wobbling mode. The triaxial deformation parameters $\varepsilon = 0.16$ and $\gamma = 26°$ are supported by tilted axis cranking calculations and the increase of the wobbling energy with spin I is attributed to nearly equal MoIs with respect to the short (s-) axis and intermediate (m-) axis ($\mathcal{J}_s \simeq \mathcal{J}_m$). The m-axis is no longer preferred for alignment with the collective rotor angular momentum $\boldsymbol{R}$, which has now a larger component along the s-axis. The mechanism underlying the enlarged $\mathcal{J}_s$-value is attributed to the gradual alignment of a pair of positive-parity (gd) protons with the s-axis. In the calculations of Ref. [15], this mechanism is taken into account by introducing a spin-dependent MoI for $\mathcal{J}_s$. Such a scenario is obviously more complex than the classification scheme suggested in Ref. [2], which assumes $\mathcal{J}_s < \mathcal{J}_m$. Therefore, the situation in ^{133}La corresponds to an intermediate coupling scheme.

Very recently, in Ref. [17] the g-factor and the static (spectroscopic) quadrupole moment (SQM) were measured for the bandhead state (an $11/2^-$ isomeric state) of the yrast band in ^{133}La. The obtained g-factor is $g = 1.16 \pm 0.07$ and the SQM is $|Q| = 1.71 \pm 0.34$ eb. On the theoretical side, Monte Carlo shell-model (MCSM) calculations gave $g = 1.16$ and provided the information that the dominant configuration of the $11/2^-$ isomeric state is $\pi(1h_{11/2})^1$. At the same time, these calculations predicted $Q = -1.25$ eb. The distribution of the quadrupole moment expectation values obtained with shell-model wave functions for the $11/2^-$ state indicates a triaxial shape with deformation parameters $\beta \sim 0.16$ and $\gamma \sim 20°$ [17], which is consistent with the wobbling interpretation. These new results motivate us to investigate the g-factor and SQM as functions of the spin I in the wobbling motion, taking the nucleus ^{133}La as a first example.

Our calculations are carried out with the particle rotor model (PRM), which has been used widely for describing wobbling bands and has achieved much success in this respect [2,4,5,10,12,14–16,18–22]. In Ref. [15], the PRM (there called "quasi-particle plus triaxial rotor model") could reproduce well the experimental energy spectra and wobbling energies together with the electromagnetic transition probability ratios, $B(M1)_{\rm out}/B(E2)_{\rm in}$ and $B(E2)_{\rm out}/B(E2)_{\rm in}$, for the wobbling bands in ^{133}La. In this work we use the same triaxial deformation parameters $\beta = 0.168$ and $\gamma = 26°$, which agree with the deformation parameters $\varepsilon = 0.16$ (here $\varepsilon = (3/2)\sqrt{5/4pi}\beta = 0.95\beta$) and $\gamma = 26°$ in Ref. [15]. With this chosen value of γ, the 1-axis, 2-axis, and 3-axis are the conventional m-axis, s-axis, and l-axis of the triaxially deformed ellipsoid, respectively. The MoIs of the nuclear core are taken as $\mathcal{J}_m = 15.33$ $\hbar^2$/MeV, $\mathcal{J}_l = 2.92$ $\hbar^2$/MeV, and $\mathcal{J}_s = [9.125 + 0.657(I - j)]$ $\hbar^2$/MeV [15]. Here, I and $j = 11/2$ are the quantum numbers related to the total angular momentum $\boldsymbol{I}$ and the proton angular momentum $\boldsymbol{j}_p$.

In the following, the methods to calculate the g-factor and SQM are given. For an odd-mass nuclear system the rotor angular momentum $\boldsymbol{R}$ and the (proton) particle angular momentum $\boldsymbol{j}_p$ are coupled to the total spin $\boldsymbol{I}$ as

$$\boldsymbol{R} + \boldsymbol{j}_p = \boldsymbol{I} \,. \tag{1}$$

The magnetic moment μ of this system is calculated from the (rotational) wave function $|I, M = I\rangle$, with M the quantum number related to the projection of $\boldsymbol{I}$ onto the z-axis of the laboratory frame, as follows

$$\mu = gI = \langle II|g\hat{I}_z|II\rangle = \langle II|g_p\hat{j}_{pz} + g_R\hat{R}_z|II\rangle \,, \tag{2}$$

where $\hat{I}_z$, $\hat{j}_{pz}$, and $\hat{R}_z$ are the z-components of the respective angular momentum operators. Moreover, g_p and g_R are the gyromagnetic ratios of the proton-particle and the core, while the output quantity g refers to the total nuclear system. In the present study, we use the values $g_R = Z/A = 0.43$ for the rotor and $g_p = 1.21$ for the $h_{11/2}$ valence-proton, in which the spin g-factor $g_s = 3.35$ has been reduced to 0.6 times that of a free proton [1]. This quenching factor is closed to the value 0.64 used in Ref. [17]. The possible modification of g_R by the (dg) quasi-proton alignment can be neglected, because the spin contribution to the g-factor is small for normal-parity single-particle states.

Using angular momentum algebra, the matrix element in Eq. (2) can be expressed through scalar products of angular momentum operators, which allows to express more directly the angular momentum geometry. The generalized Landé formula reads

$$\mu = gI = \frac{\langle II|g_p\boldsymbol{j}_p\cdot\boldsymbol{I} + g_R\boldsymbol{R}\cdot\boldsymbol{I}|II\rangle}{I(I+1)}I \,. \tag{3}$$

By means of Eq. (1) the expression for the g-factor of the total nuclear system can be rearranged such that it depends on the expectation values of the relative orientations between $\boldsymbol{j}_p$, $\boldsymbol{R}$, and $\boldsymbol{I}$,

$$g = \frac{\langle g_p\boldsymbol{j}_p\cdot\boldsymbol{I} + g_R\boldsymbol{R}\cdot\boldsymbol{I}\rangle}{I(I+1)} \tag{4}$$

$$= g_R + (g_p - g_R)\frac{\langle\boldsymbol{j}_p\cdot\boldsymbol{I}\rangle}{I(I+1)} \tag{5}$$

$$= g_R + (g_p - g_R)\frac{j(j+1)}{I(I+1)} + (g_p - g_R)\frac{\langle\boldsymbol{j}_p\cdot\boldsymbol{R}\rangle}{I(I+1)} \tag{6}$$

$$= \frac{1}{2}\Big[(g_p + g_R) + (g_p - g_R)\frac{j(j+1) - \langle\boldsymbol{R}^2\rangle}{I(I+1)}\Big] \,. \tag{7}$$

As limiting cases, one obtains

- $g = g_R$, in the case $\boldsymbol{j}_p \perp \boldsymbol{I}$;
- $g = g_R + (g_p - g_R)\sqrt{\frac{j(j+1)}{I(I+1)}}$, in the case $\boldsymbol{j}_p \parallel \boldsymbol{I}$;
- $g = g_R + (g_p - g_R)\frac{j(j+1)}{I(I+1)}$, in the case $\boldsymbol{j}_p \perp \boldsymbol{R}$.

It is worth mentioning here that the g-factor has been used to investigate the angular momentum coupling scheme in chiral doublet bands in Refs. [23,24]. According to Eq. (7), one can get from the g-factor also information about the rotor angular momentum, via the expectation value $\langle\boldsymbol{R}^2\rangle$.

The SQM gives a measure of the nuclear charge distribution associated with the collective rotational motion, and it is calculated as [1,25]

$$Q(I) = \langle II|\hat{Q}_{20}|II\rangle \,, \tag{8}$$

where the quadrupole moment operator in the laboratory frame $\hat{Q}_{20}$ is obtained from the intrinsic quadrupole moments $Q'_{2\nu}$ by multiplication with Wigner D-functions:

$$\hat{Q}_{20} = \sum_\nu D^2_{0,\nu}Q'_{2\nu} \,. \tag{9}$$

The three (non-vanishing) intrinsic quadrupole moments are

$$Q'_{20} = Q'_0\cos\gamma, \quad Q'_{22} = Q'_{2-2} = Q'_0\sin\gamma/\sqrt{2}, \tag{10}$$

$$Q'_0 = 3R_0^2Z(\beta + 0.16\beta^2)/\sqrt{5\pi}, \tag{11}$$

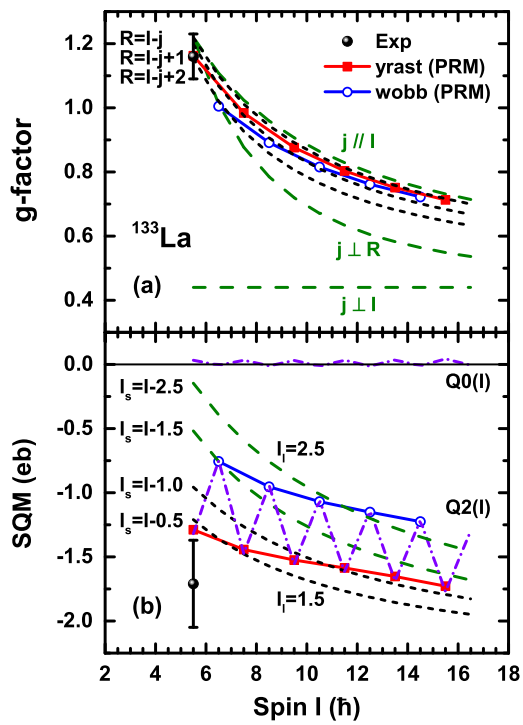

Fig. 1. g-factors (a) and static quadrupole moments (b) as functions of the spin I calculated in the PRM for the yrast and wobbling bands in ^{133}La in comparison to the available data [17]. (a) The dashed lines correspond to parallel and perpendicular couplings of the angular momenta of the proton and rotor. The short dashed lines represent the formula in Eq. (7), evaluated with different rotor angular momentum quantum numbers: $R = I - j$, $I - j + 1$, and $I - j + 2$. (b) The dashed-dot lines for $Q_0(I)$ and $Q_2(I)$ follow from Eqs. (13) and (14). The dashed and short-dashed lines show $Q_2(I)$ calculated by Eq. (14) using the values of I_s and I_l as specified in the figure.

with Z the proton number and $R_0 = 1.2\,\mathrm{fm}\,A^{1/3}$. The SQM values are obtained by evaluating Eqs. (8)-(9) with the PRM wave functions, where the triaxial deformation parameters $\beta = 0.168$ and $\gamma = 26°$ are used in the PRM calculations.

In order to demonstrate the dependence of the SQM on the geometry of the angular momentum vectors, we follow Ref. [26], where it was shown that the SQM formula (8) can be expressed in terms of the expectation values of the squared total angular momentum components along the three principal axes $\langle \hat{I}_k^2 \rangle$,

$$Q(I) = Q_0(I) + Q_2(I)\,, \tag{12}$$

$$Q_0(I) = \frac{3\langle \hat{I}_3^2 \rangle - I(I+1)}{(I+1)(2I+3)} Q_0' \cos\gamma\,, \tag{13}$$

$$Q_2(I) = \frac{\sqrt{3}(\langle \hat{I}_1^2 \rangle - \langle \hat{I}_2^2 \rangle)}{(I+1)(2I+3)} Q_0' \sin\gamma\,. \tag{14}$$

In this way, the SQM provides direct information about the orientation of the total angular momentum relative to the principal axes frame.

In Fig. 1, we show the g-factor and SQM as functions of the spin I as calculated in the PRM for states in the yrast and wobbling bands of ^{133}La in comparison with the available experimental data [17].

The PRM reproduces well the experimental g-factor at the head of the yrast band. The theoretical prediction $g = 1.16$ is in excellent agreement with the experimental value $g = 1.16 \pm 0.07$. The calculated g-factors decrease with increasing spin I. This feature comes mainly from the denominator $I(I+1)$ in Eqs. (5)-(7), because $g_p - g_R = 0.78$ is positive. Over the entire spin region the g-factors for states in the yrast band are larger than those for states in the wobbling band. According to Eq. (7), this suggests that the expectation value of the rotor angular momentum $\langle \boldsymbol{R}^2 \rangle$ is smaller in the yrast band than in the wobbling band, since $g_p - g_R$ is positive. In the following, we will see that this behavior is induced by a wobbling motion.

In Fig. 1(a), we also show the g-factors as functions of I for the limiting cases $\boldsymbol{j}_p \perp \boldsymbol{I}$, $\boldsymbol{j}_p \parallel \boldsymbol{I}$, and $\boldsymbol{j}_p \perp \boldsymbol{R}$. One can observe that for $\boldsymbol{j}_p \parallel \boldsymbol{I}$ the g-factor is quite close to the results obtained in the yrast and wobbling bands, whereas for $\boldsymbol{j}_p \perp \boldsymbol{I}$ it lies far away. At the bandhead the limiting cases $\boldsymbol{j}_p \perp \boldsymbol{R}$ and $\boldsymbol{j}_p \parallel \boldsymbol{I}$ are close because R is small there. This indicates the angular momenta of the proton $\boldsymbol{j}_p$ and total nuclear system $\boldsymbol{I}$ are oriented almost parallel to each other in the yrast and wobbling bands. For illustration we present also the g-factor according to Eq. (7) with $\langle \boldsymbol{R}^2 \rangle = R(R+1)$, taking rotor angular momentum quantum numbers: $R = I - j$, $R = I - j + 1$, and $R = I - j + 2$. One sees that the curve with $R = I - j + 2$ agrees best with the experimental values at $I = 11/2$, which indicates that the rotor angular momentum is close to $R = 2$ at the bandhead. For higher spins I the curves $R = I - j$ and $R = I - j + 1$ agree better with experimental values in the yrast and wobbling bands, respectively.

At $I = 11/2$ the calculated SQM $Q(11/2) = -1.29$ eb comes out close to upper limit of the experimental value $Q(11/2) = -1.71 \pm 0.34$ eb. This reasonable agreement indicates that calculations in the PRM correctly account for the structure of the collective (rotational) states. The calculated SQM decreases with increasing spin I as a consequence of the denominator $(I+1)(2I+3)$ in Eqs. (13)-(14). We note that the more sophisticated MCSM calculations in Ref. [17] give $Q(11/2) = -1.25$ eb. Using the deformation parameter $\beta = 0.22$ in the PRM calculations, which is a somewhat larger than our value of $\beta = 0.168$ from self-consistent mean field calculations, shifts $Q(11/2)$ in Fig. 1 into the center of the experimental interval and does not change significantly its spin dependence (see below).

In Fig. 1(b) the contributions $Q_0(I)$ and $Q_2(I)$ as calculated by Eqs. (13) and (14) are shown separately. In the evaluation $\gamma = 240° + 26°$ is used instead of $\gamma = 26°$, which corresponds to the same shape, however a different assignment of the principal axes: $1 \to s$, $2 \to l$, $3 \to m$. The advantage of this choice is that $\cos 270° = 0$ and $\sin 270° = -1$, which simplifies the discussion for nearby γ-values. Accordingly, $Q_0(I)$ is almost zero, since it gets strongly suppressed by the factor $\cos 266° = -0.07$. Hence, $Q_2(I) \simeq Q(I)$ which is shown in the lower part of Fig. 1(b) for the following root-mean-square expectation values of total angular components $I_i = \langle \hat{I}_i^2 \rangle^{1/2}$ along the s-axis and l-axis: $(I_s, I_l) = (I - 1/2, 3/2)$, $(I - 1, 3/2)$, $(I - 3/2, 5/2)$, and $(I - 5/2, 5/2)$. The former two and latter two curves agree with the experimental results for states in the yrast and wobbling bands, respectively. Clearly, the I_s values in the yrast band are larger than those in the wobbling band. We shall see that this feature is again caused by the wobbling motion. Altogether, the values $Q_2(I) \simeq Q(I)$ are smaller for states in the yrast band than in the wobbling band. As $\sin 266° = -0.99$, the negative values of the SQMs are caused by the fact that the total angular momentum $\boldsymbol{I}$ aligns mainly along the s-axis. The PRM gives for the $I = 11/2$ state $\langle \hat{I}_s^2 \rangle = 26.80$, $\langle \hat{I}_l^2 \rangle = 1.97$, $\langle \hat{I}_m^2 \rangle = 6.98$. Using these values in Eqs. (13)-(14) and $\beta = 0.22$ shifts the SQM to -1.70 eb, in agreement with the experimental value.

The authors of Ref. [17] assumed prolate shape. In this case, the SQM is

$$Q(I) = \frac{3K^2 - I(I+1)}{(I+1)(2I+3)} Q_0'\,. \tag{15}$$

Using this formula under the assumption $K = 1/2$ they extracted a deformation parameter of $\beta = 0.28 \pm 0.10$ from the measured SQM

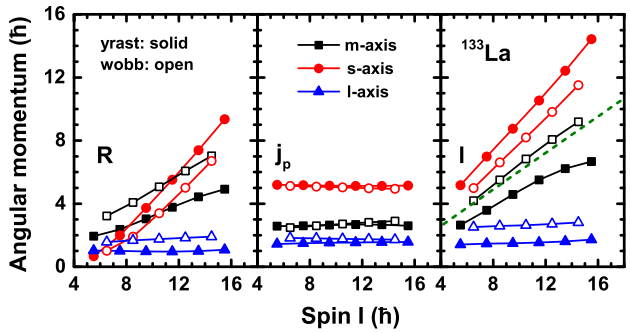

Fig. 2. Angular momentum components along the intermediate (m-), short (s-), and long (l-) axis of the rotor, proton-particle, and total nuclear system as functions of the spin I for the yrast and wobbling bands in ^{133}La. Each component is a root-mean-square expectation value of an angular momentum operator, e.g. $I_s = \langle \hat{I}_s^2 \rangle^{1/2}$. The dashed lines correspond to the average quantity $\sqrt{I(I+1)/3}$.

$|Q| = 1.71 \pm 0.34$ eb for the $11/2^-$ isomeric state at the bandhead of ^{133}La, which is unusually large for low-lying states in this mass region. As discussed, taking triaxility into account brings β down to 0.22, a value more typical to the $A \sim 130$ mass region. It would be interesting to determine the deformation independently by measuring the lifetimes of the rotational states.

In order to better understand the behavior of the g-factor and SQM as functions of the spin I, we will discuss in the following the angular momentum geometry of the proton-particle and the collective rotor.

In Fig. 2, we present the calculated angular momentum components along the m-, s-, and l-axis of the rotor ($\boldsymbol{R}$), proton-particle ($\boldsymbol{j}_p$), and total nuclear system ($\boldsymbol{I}$) as functions of the spin I for the yrast and wobbling bands in ^{133}La. The proton angular momentum $\boldsymbol{j}_p$ aligns mainly with the s-axis, because its torus-like orientational probability distribution has a maximal overlap with the triaxial nuclear core in the ml-plane [27]. The s-component is constant $j_s \simeq 5$ over the whole spin region for both the yrast and the wobbling band. The rotor angular momentum $\boldsymbol{R}$ favors a location in the sm-plane with a very small l-component, because $\mathcal{J}_l$ is the smallest. With increasing spin I, R_s increases faster than R_m, due to the gradual increase of $\mathcal{J}_s$. This behavior of $\boldsymbol{R}$ combined with $\boldsymbol{j}_p$ makes I_s being largest. The latter feature leads to the negative values of $Q_2(I)$ as shown in Fig. 1(b). In addition, the component I_s (I_m) for states in the yrast band is larger (smaller) than for those in the wobbling band. A wobbling motion takes place about the s-axis, as it also occurs in the neighboring isotone ^{135}Pr [9,10]. The enhanced magnitude of R_s, due to the increase of $\mathcal{J}_s$, stabilizes the wobbling motion about s-axis. This fact is consistent with increasing wobbling energies [15]. Since $\mathcal{J}_s$ and $\mathcal{J}_m$ are almost equal, a classification of the wobbling mode as longitudinal or transverse seems inappropriate. The angular momentum geometry is just more complex, corresponding to an intermediate situation between the two limits.

Moreover, the component I_m is close to the average quantity $\sqrt{I(I+1)/3}$. This explains why the contribution $Q_0(I)$ vanishes almost, as shown in Fig. 1(b). The component I_l is small, with a value $I_l \approx 3/2$ for the yrast band and $I_l \approx 5/2$ for the wobbling band. This explains why the outcome of the analytical formula for $Q_2(I)$ in Eq. (14) agrees so well with the full calculation in the PRM for yrast and wobbling bands.

In order to illustrate further the wobbling motion about the s-axis, the probability density distributions $\mathcal{P}(\theta, \varphi)$ for the orientation of the total angular momentum $\boldsymbol{I}$ on the $\theta\varphi$-sphere (called azimuthal plots [21,28–30]) are shown in Fig. 3 for states in the yrast and wobbling bands of ^{133}La. Here, θ is a polar angle between the total spin $\boldsymbol{I}$ and the l-axis, and φ is an azimuthal angle in the sm-plane measured from the s-axis. Over the entire spin region,

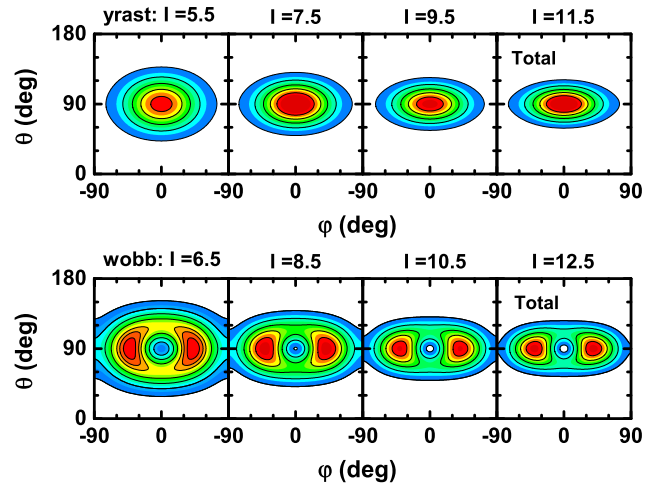

Fig. 3. Azimuthal plots, i.e., probability density distributions for the orientation of the angular momentum $\boldsymbol{I}$ on the $\theta\varphi$-sphere as calculated in the PRM for states in the yrast and wobbling bands of ^{133}La.

the distributions $\mathcal{P}(\theta, \varphi)$ are centered about $\theta = 90°$, which corresponds to very small I_l-components, as shown earlier in Fig. 2. For states in the yrast band the maximum lies at $\varphi = 0°$, which represents a highest probability of aligning $\boldsymbol{I}$ along the s-axis. To the contrary, states in the wobbling band have a minimum at $\varphi = 0$. For these wobbling states, the maximal probability lies on a rim around the minimum, and $\mathcal{P}(\theta, \varphi)$ reflects in this way the wobbling motion (or precession) of $\boldsymbol{I}$ about the s-axis. Note that one obtains here precisely the distributions as expected for the wobbling motion [12,21], namely φ-symmetric wave functions for the ($n = 0$) yrast band and φ-antisymmetric wave functions for the ($n = 1$) wobbling band. Moreover, the feature that the distributions centered at $\varphi = 0°$ do not extend out to $\varphi = \pm 90°$ indicates that the wobbling mode in ^{133}La is very stable, which is guaranteed by a gradual increase of $\mathcal{J}_s$ with I.

In Fig. 4, we show the calculated probability distributions for the rotor angular momentum (R-plots P_R, a1-a2), for the projection of the rotor angular momentum onto the m-axis (K_R-plots P_{R_m}, b1-b2), and for the projection of the total angular momentum onto the s-axis (K-plots P_{I_s}, c1-c2), in the yrast and wobbling bands of ^{133}La. These detailed results do further support the picture of a wobbling motion about the s-axis.

The R-plots (a1) and (a2) show a similar behavior as those for the nucleus ^{135}Pr [21], namely, for states in the yrast band R is almost a good quantum number. The P_R-distributions have a pronounced peak at $R = I - j$, except for the bandhead with $I = 11/2$, where the maximal weight occurs at $R = I - j + 2 = 2$. For states in the wobbling band an admixture of substates with $R = I - j$ and $R = I - j + 1$ is present. An exception occurs again at the bandhead $I = 13/2$, where the peaks lie at $R = I - j + 1$ and $I - j + 3$. According to these characteristics, one can understand the behavior of the g-factor as a function of spin I, as shown in Fig. 1(a).

The K_R-plots (b1) and (b2) illustrate how the picture of a wobbling oscillation arises. The distributions P_{R_m} display large admixtures of various values of R_m, which have their origin in the wobbling motion of the rotor towards to the m-axis. At $R_m = 0$, the distribution P_{R_m} has a finite value for states in the yrast band, while it vanishes for states in the wobbling band. This is a characteristic of the one-phonon excitation of the wobbling mode and it is consistent with φ-symmetric wave functions for ($n = 0$) yrast states and φ-antisymmetric wave functions for ($n = 1$) wobbling states, as visualized by the azimuthal plots $\mathcal{P}(\theta, \varphi)$ in Fig. 3.

The K-plots (c1) and (c2) display that the prominent peaks of the distribution P_{I_s} appear at $I_s = \pm I$ for states in the yrast band,

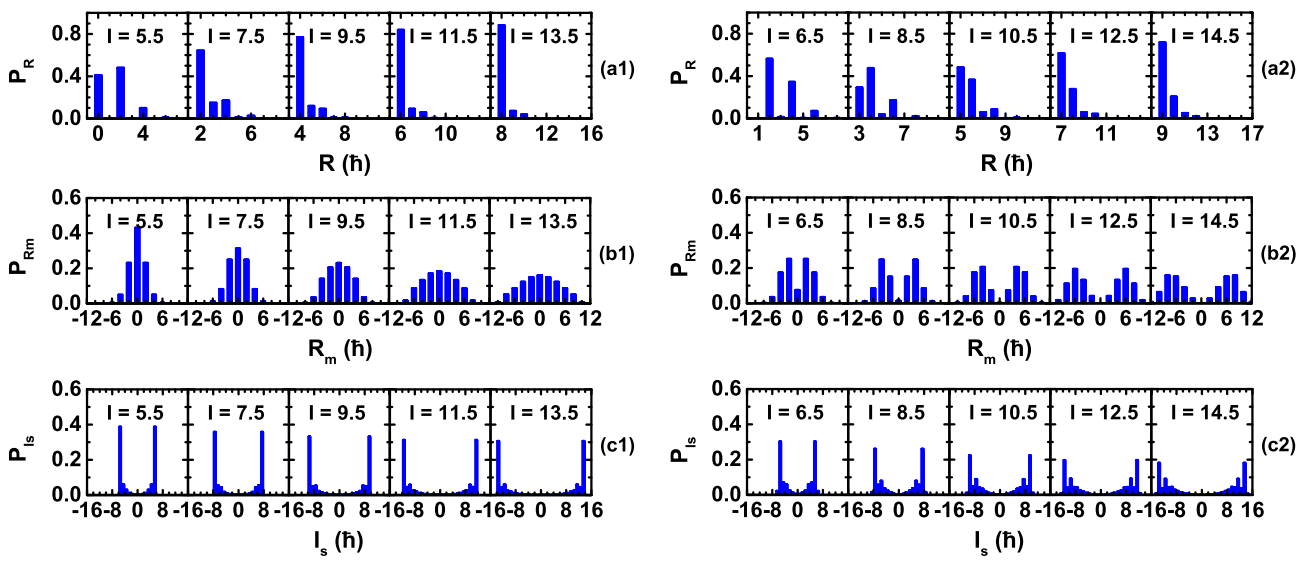

Fig. 4. Probability distributions for the rotor angular momentum (R-plot P_R, a1-a2), for the projection of the rotor angular momentum onto the m-axis (K_R-plot P_{R_m}, b1-b2), and for the projection of the total angular momentum onto the s-axis (K-plot P_{I_s}, c1-c2) as calculated in the PRM for states in the yrast and wobbling bands of ^{133}La.

and at $I_s = \pm(I-1)$ for states in the wobbling band. This corresponds to the classical picture of the wobbling motion. The yrast state with spin I and the neighboring wobbling state with spin $I+1$ have similar angular momentum components along the s-axis. The total angular momentum in a wobbling state with $I+1$ has to precess (wobble) with respect to s-axis to reach $I_s \simeq I$.

In summary, the g-factor and SQM for the wobbling mode of ^{133}La have been investigated in the framework of the PRM. The calculation reproduces the available g-factor and SQM data well. The properties of the g-factor and SQM as functions of spin I have been interpreted by analyzing the angular momentum components of the rotor, proton-particle, and total nuclear system with the help of various quantum mechanical probability distributions: azimuthal plots, R-plots, K_R-plots, and K-plots. It has been demonstrated that the wobbling mode in ^{133}La corresponds to a wobbling of $\boldsymbol{I}$ about the s-axis. The g-factor at the bandhead of yrast band gives the information $R \simeq 2$ about the rotor angular momentum $\boldsymbol{R}$. The variation of the g-factor with spin I indicates that the angular momenta of the proton-particle and total nuclear system are oriented parallel to each other. The negative values of the SQMs are caused by the fact that the total angular momentum $\boldsymbol{I}$ aligns with the s-axis. The differences of the SQM between states in the yrast and wobbling bands can be traced back to the wobbling motion. Therefore, the g-factor and SQM are good indicators of the angular momentum geometry for the wobbling motion. Future experimental measurements of g-factors and the SQMs for states in the high-spin region are strongly suggested in order to test the theoretical predictions presented in this work.

Declaration of competing interest

The authors declare that they have no known competing financial interests or personal relationships that could have appeared to influence the work reported in this paper.

Acknowledgements

This work has been supported in parts by Deutsche Forschungsgemeinschaft (DFG) and National Natural Science Foundation of China (NSFC) through funds provided by the Sino-German CRC 110 “Symmetries and the Emergence of Structure in QCD” (DFG Grant No. TRR110 and NSFC Grant No. 11621131001), the US Department of Energy (Grant No. DE-FG02-95ER40934), the National Key R&D Program of China (Contract No. 2017YFE0116700 and No. 2018YFA0404400), the NSFC under Grant No. 11935003, and the State Key Laboratory of Nuclear Physics and Technology of Peking University (Grant No. NPT2020ZZ01). The work of U.-G.M. was also supported by the Chinese Academy of Sciences (CAS) through a President’s International Fellowship Initiative (PIFI) (Grant No. 2018DM0034) and by the VolkswagenStiftung (Grant No. 93562).

References

[1] A. Bohr, B.R. Mottelson, Nuclear Structure, vol. II, Benjamin, New York, 1975.
[2] S. Frauendorf, F. Dönau, Phys. Rev. C 89 (2014) 014322.
[3] P. Bringel, G.B. Hagemann, H. Hübel, A. Al-khatib, P. Bednarczyk, A. Bürger, D. Curien, G. Gangopadhyay, B. Herskind, D.R. Jensen, et al., Eur. Phys. J. A 24 (2005) 167.
[4] S.W. Ødegård, G.B. Hagemann, D.R. Jensen, M. Bergström, B. Herskind, G. Sletten, S. Törmänen, J.N. Wilson, P.O. Tjøm, I. Hamamoto, et al., Phys. Rev. Lett. 86 (2001) 5866.
[5] D.R. Jensen, G.B. Hagemann, I. Hamamoto, S.W. Ødegård, B. Herskind, G. Sletten, J.N. Wilson, K. Spohr, H. Hübel, P. Bringel, et al., Phys. Rev. Lett. 89 (2002) 142503.
[6] G. Schönwaßer, H. Hübel, G.B. Hagemann, P. Bednarczyk, G. Benzoni, A. Bracco, P. Bringel, R. Chapman, D. Curien, J. Domscheit, et al., Phys. Lett. B 552 (2003) 9.
[7] H. Amro, W.C. Ma, G.B. Hagemann, R.M. Diamond, J. Domscheit, P. Fallon, A. Gorgen, B. Herskind, H. Hübel, D.R. Jensen, et al., Phys. Lett. B 553 (2003) 197.
[8] D.J. Hartley, R.V.F. Janssens, L.L. Riedinger, M.A. Riley, A. Aguilar, M.P. Carpenter, C.J. Chiara, P. Chowdhury, I.G. Darby, U. Garg, et al., Phys. Rev. C 80 (2009) 041304(R).
[9] J.T. Matta, U. Garg, W. Li, S. Frauendorf, A.D. Ayangeakaa, D. Patel, K.W. Schlax, R. Palit, S. Saha, J. Sethi, et al., Phys. Rev. Lett. 114 (2015) 082501.
[10] N. Sensharma, U. Garg, S. Zhu, A.D. Ayangeakaa, S. Frauendorf, W. Li, G. Bhat, J.A. Sheikh, M.P. Carpenter, Q.B. Chen, et al., Phys. Lett. B 792 (2019) 170.
[11] C.M. Petrache, P.M. Walker, S. Guo, Q.B. Chen, S. Frauendorf, Y.X. Liu, R.A. Wyss, D. Mengoni, Y.H. Qiang, A. Astier, et al., Phys. Lett. B 795 (2019) 241.
[12] Q.B. Chen, S. Frauendorf, C.M. Petrache, Phys. Rev. C 100 (2019) 061301(R).
[13] Y.K. Wang, F.Q. Chen, P.W. Zhao, Phys. Lett. B 802 (2020) 135246.
[14] J. Timár, Q.B. Chen, B. Kruzsicz, D. Sohler, I. Kuti, S.Q. Zhang, J. Meng, P. Joshi, R. Wadsworth, K. Starosta, et al., Phys. Rev. Lett. 122 (2019) 062501.
[15] S. Biswas, R. Palit, S. Frauendorf, U. Garg, W. Li, G.H. Bhat, J.A. Sheikh, J. Sethi, S. Saha, P. Singh, et al., Eur. Phys. J. A 55 (2019) 159.
[16] N. Sensharma, U. Garg, Q.B. Chen, S. Frauendorf, D.P. Burdette, J.L. Cozzi, K.B. Howard, S. Zhu, M.P. Carpenter, P. Copp, et al., Phys. Rev. Lett. 124 (2020) 052501.
[17] M.S.R. Laskar, R. Palit, S.N. Mishra, N. Shimizu, Y. Utsuno, E. Ideguchi, U. Garg, S. Biswas, F.S. Babra, R. Gala, et al., Phys. Rev. C 101 (2020) 034315.
[18] I. Hamamoto, Phys. Rev. C 65 (2002) 044305.
[19] I. Hamamoto, B.R. Mottelson, Phys. Rev. C 68 (2003) 034312.

[20] W.X. Shi, Q.B. Chen, Chin. Phys. C 39 (2015) 054105.
[21] E. Streck, Q.B. Chen, N. Kaiser, U.-G. Meißner, Phys. Rev. C 98 (2018) 044314.
[22] Q.B. Chen, N. Kaiser, U.-G. Meißner, J. Meng, arXiv:2003.04065 [nucl-th].
[23] S. Frauendorf, J. Meng, Nucl. Phys. A 617 (1997) 131.
[24] E. Grodner, J. Srebrny, C. Droste, L. Próchniak, S.G. Rohoziński, M. Kowalczyk, M. Ionescu-Bujor, C.A. Ur, K. Starosta, T. Ahn, et al., Phys. Rev. Lett. 120 (2018) 022502.
[25] P. Ring, P. Schuck, The Nuclear Many Body Problem, Springer Verlag, Berlin, 1980.
[26] Q.B. Chen, N. Kaiser, U.-G. Meißner, J. Meng, Phys. Lett. B 807 (2020) 135568.
[27] S. Frauendorf, J. Meng, Z. Phys. A 356 (1996) 263.
[28] F.Q. Chen, Q.B. Chen, Y.A. Luo, J. Meng, S.Q. Zhang, Phys. Rev. C 96 (2017) 051303(R).
[29] F.Q. Chen, J. Meng, S.Q. Zhang, Phys. Lett. B 785 (2018) 211.
[30] Q.B. Chen, J. Meng, Phys. Rev. C 98 (2018) 031303(R).
[31] http://www.nndc.bnl.gov/ensdf/.